MRS Communications (2016), 6, 85–91
© Materials Research Society, 2016
doi:10.1557/mrc.2016.10

MRS Communications

Research Letters

Local-structure-affected behavior during self-driven grain boundary migration

X. M. Luo, Shenyang National Laboratory for Materials Science, Institute of Metal Research, Chinese Academy of Sciences, 72 Wenhua Road, Shenyang 110016, People's Republic of China
B. Zhang, Key Laboratory for Anisotropy and Texture of Materials, Ministry of Education, School of Materials Science and Engineering, Northeastern University, 3-11 Wenhua Road, Shenyang 110819, People's Republic of China
X. F. Zhu, and **Y. T. Zhou,** Shenyang National Laboratory for Materials Science, Institute of Metal Research, Chinese Academy of Sciences, 72 Wenhua Road, Shenyang 110016, People's Republic of China
T. Y. Xiao, Key Laboratory for Anisotropy and Texture of Materials, Ministry of Education, School of Materials Science and Engineering, Northeastern University, 3-11 Wenhua Road, Shenyang 110819, People's Republic of China
G. P. Zhang, Shenyang National Laboratory for Materials Science, Institute of Metal Research, Chinese Academy of Sciences, 72 Wenhua Road, Shenyang 110016, People's Republic of China

Address all correspondence to G. P. Zhang at **gpzhang@imr.ac.cn**

(Received 29 November 2015; accepted 25 February 2016)

Abstract

In nanocrystalline (nc) metals, it is still not clear how local grain boundary (GB) structures accommodate GB migration at atomic scales and what dominates the motion of atoms at the inherently unstable GB front. Here, we report the adjustment of the local GB structures at atomic scales during self-driven GB migration, simultaneously involving GB dissociation, partial dislocation emission from GB, and faceting/defaceting in the nc Cu. Furthermore, we reveal that the fundamental of GB migration ability is closely related to the local structure, i.e. the GB segment consisting of "hybrid" structural units and delocalized GB dislocations is relatively unstable.

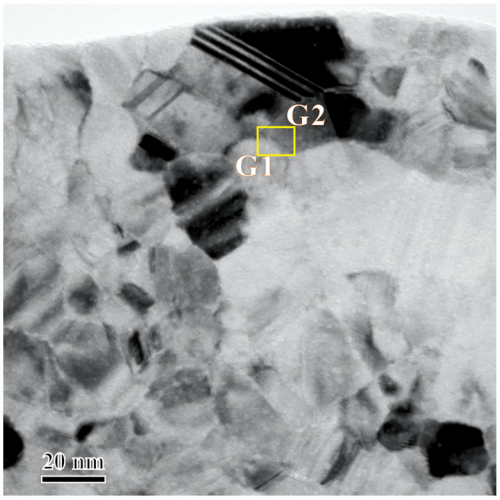
Nanocrystalline (nc) materials, showing unusual mechanical properties (dramatically increased strength and hardness,[1,2] and even greatly enhanced ductility[3]), have great technological attraction. However, grain boundaries (GBs) usually become unstable, and GB-related deformation takes over in nc materials.[2,4] The GB-related behaviors are found to operate by three main processes: GB migration,[4,5] dislocation nucleation from GB,[6] and GB dislocation (GBD) motion.[7] GB migration may happen simultaneously accompanying with other GB-related behaviors. Molecular dynamics simulations[8] and experimental observations[9] suggest that twin lamella can form via GB migration or dissociation. GBs containing GBDs can emit a partial dislocation during deformation by local atomic shuffling and stress-assisted free volume migration.[10,11] Simultaneously, GB-related behaviors also greatly change the local GB environment. GB ledges were observed to form by the glide motion of dislocations in the GB plane.[12] GB migration would form periodic facets.[13] Obviously, the interaction among different GB-related behaviors is a very complex process, which needs to be gotten insight into.

As a useful tool for studying GB, high-resolution transmission electron microscope (HRTEM) observation has been performed on thermal-activated [110] tilt GB motion,[14] surface energy-driven twist and general GB motion,[15,16] and stress-driven incoherent twin boundary (TB) motion.[17] Although considerable progress has been made in understanding GB migration and other GB-related behaviors, the underlying atomic-scale mechanisms are still less known, especially when GB migration involves other GB-related behaviors.[14,18]

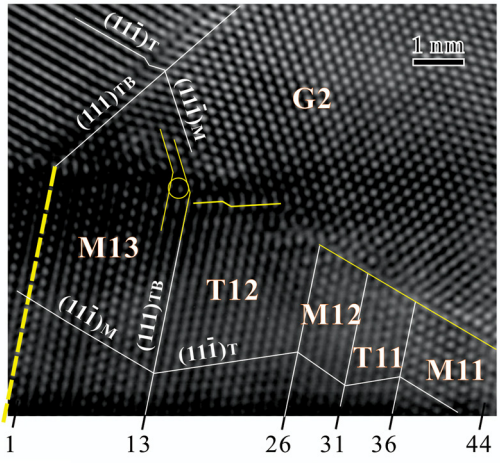
In this study, through in situ HRTEM investigations, we reveal the GB local structure adjustment at atomic scales during self-driven GB migration under electron irradiation, simultaneously involving partial dislocation emission, GBD motion, GB dissociation and faceting/defaceting. Based on the GB structural unit model, we uncover some interaction of the local GB structures and quantitative GB-related behaviors, which are closely related to the GB migration ability.

The 50 nm-thick copper film (target purity: 99.999%) was deposited onto a 125-μm-thick polyimide substrate under high-vacuum conditions (base pressure $< 1 \times 10^{-4}$ Torr) using DC magnetron sputtering. Before the deposition, the substrate was sputtering cleaned by Ar^+ at a power of 50 W and a pressure of 0.4 Pa for about 5 min. The samples for HRTEM and transmission electron microscope (TEM) investigations were mechanically ground to ~30 μm in thickness, and then further thinned by ion milling on a precision ion polishing system (Gatan 691) at −100 °C. The final low-angle (2°) and low-energy (2 kV) ion mills were selected to minimize potential contamination and surface damage.

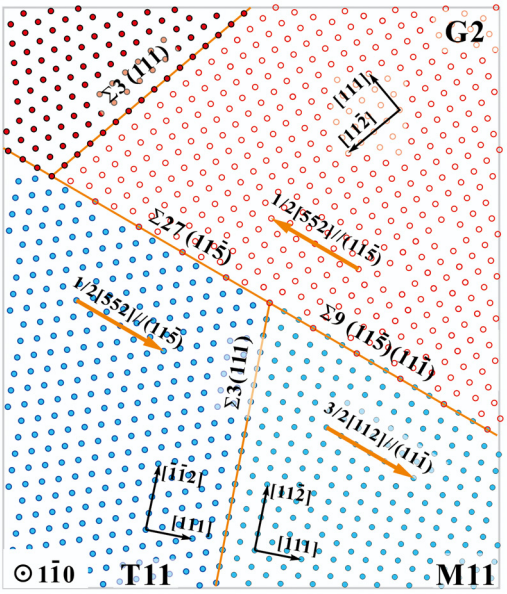
https://doi.org/10.1557/mrc.2016.10 Published online by Cambridge University Press



(a)



(b)



(c)

HRTEM observations were performed in a field emission gun TEM (FEI Tecnai F20) operated at 200 kV and the current density ~4.8 A/cm^2. Image sequences at magnifications of 1,050,000× were recorded with a 0.5-s interval by a Gatan image intensified camera. To eliminate possible artifacts during interpretation of the dislocation analysis, HRTEM simulations were carried out using the multislice method as implemented in the QSTEM program.[19]

Results

A TEM micrograph [Fig. 1(a)] indicates that initial microstructure of the copper film consists of nanograins with a size ranging from 5 to 42 nm. Here, we focused on two nanograins **G1** and **G2** with a size of about 16 and 40 nm, respectively. The characterization [Fig. 1(b)] on the twin relationship between **G1** and **G2** shows that nanotwins exist in **G1**, and their TBs were indicated by atom arrays, namely No. 13, 26 31, and 36. The formation of the twins in G1 would cause the local misorientation variation between **G1** and **G2**. As shown in Fig. 1 (b), the misorientation angles between **M11** (or **M12, M13**) and **G2, T11** (or **T12**) and **G2** are 36.8° [$1\bar{1}0$] and 33.7° [$1\bar{1}0$], respectively. According to the Brandon criterion,[20] they are close to Σ9 and Σ27 coincidence misorientations, respectively. Thus, we describe the apparent GB structure schematically in Fig. 1(c), which exhibits an equilibrium triple junction Σ9–Σ3–Σ27. Furthermore, we found four GB facets at the macroscopically curved **G1**/**G2** GB, which consist of two $(1\,1\bar{5})/(1\,1\bar{1})$ asymmetric tilt GBs (ATGB), a stepped $(\bar{3},\bar{3},1\,1)/(1\,1\bar{1})$ ATGB and a $(1\,1\bar{5})$ symmetric tilt GB (STGB), as shown in Figs. 1(b) and 1(c).

Tens of seconds later in the HRTEM, the GB started to migrate from **G1** toward **G2**, as shown in Fig. 2(b) for 20 s and Fig. 2(c) for 26 s. Figure 2(d) depicts the variation of the GB migrating front with the time (t), revealing that the migrating distance of different parts of the GB is quite different. Thus, we separate the **G1**/**G2** GB into three segments I, II, and III. GB segment I has an obvious migration distance, while the GB segment III is quite stable. In addition, six GBDs defined by the coherence across the GB between the (111) planes[10] are also observed, as indicated by numbered solid circles in Fig. 2(d), showing the evolution of the GBDs with the GB segment moving into **G2**.

During GB migration, local GB structures experienced readjustment through a series of GB-related behaviors. GB

Figure 1. Microscopy and schematic images of the HRTEM observation: (a) Initial in-plane TEM image of the copper film. (b) HRTEM observation on the framed area between grains G1 and G2 in (a). The twin relationship and GB facets are indicated by the white and yellow lines, respectively. T11 and M11 have a twin relationship in G1. The circle indicates GBD. The thick yellow dashed line is the reference line. (c) Schematic illustration of ideal coincidence misorientations orientation Σ9 and Σ27 and observation in (b). We measure the indices of the crystalline directions indicated by the arrows, based on the coordinate axes in G1, T11, and M11. Then, we can get the plane whose projection on $(1\bar{1}0)$ plane is the arrow-indicated crystalline direction.

https://doi.org/10.1557/mrc.2016.10 Published online by Cambridge University Press

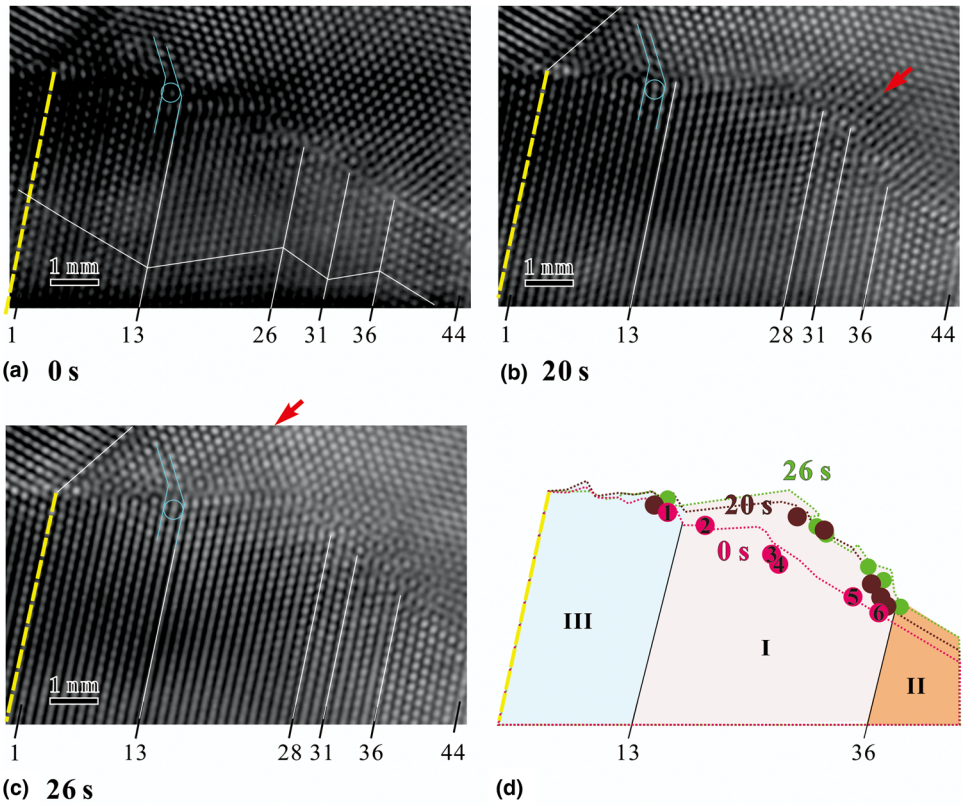


Figure 2. Microscopy and schematic images of the in situ observation: A sequence of HRTEM images, showing the variation in GB positions at different time of (a) 0 s, (b) 20 s, and (c) 26 s. The GBDs identified by the coherence of the (111) plane across the GBs are indicated by the circles. The newly formed twin is indicated by an arrow. (c) Schematic illustration of the migrating distance of the GB segments I, II, and III. The positions of the six numbered GBDs in the GBs are shown in (d).

dissociation and partial dislocation emission from the GB were observed. Comparing the initial GB structures [Fig. 2(a)] with those after GB migration [Fig. 2(b) for $t = 20$ s], the TB (No. 26) in **G1** had shifted to the atom array No. 28. Meanwhile, a two-atom-layer thick twin indicated by an arrow in Fig. 2(b) formed in **G2** through the fact that two Shockley partial dislocations were emitted along two adjacent (111) planes from the GB [see the close observation in Fig. 3(a)]. A simulated image is given in Fig. 3(b), which matches well with the experimental image. According to the Burgers circuit (FS/RH convention[21]), the total vector of the twinning partials was $(a/6)[\bar{1}\bar{1}2]$ [see Fig. 3(c)]. Thus, the two twinning partials had different Burgers vectors, here we take $b_1 = (a/6)[1\bar{2}1]$, $b_2 = (a/6)[\bar{2}11]$, and $b_1 + b_2 = (a/6)[\bar{1}\bar{1}2]$. When these partial dislocations approached the GB, they were absorbed by the GB, leading to the rearrangement of the atoms at the GB in the process of GB migration. Meanwhile, with detwinning/twinning in **G1** and **G2**, the original Σ9 GB segment was dissociated into a quadrangle region bounded by three coherent TBs, as indicated by three arrows in Fig. 3(a), and one incoherent TB in front of the twin. Such dissociation $\Sigma 9 = \Sigma 3 + \Sigma 3$ is essentially an energy-reduction process.[16,22] With further GB migration [Fig. 2(c) for $t = 26$ s], the GBD1 circled in Fig. 2(b) moved toward the triple junction and hardly advanced further due to the block of the well-ordered facet [Fig. 2(c)], and then caused another partial dislocation to emit from the junction which left behind a stacking fault, as shown in the enlarged image in Fig. 3(d) and the simulated image Fig. 3(e).

To uncover the physical origin for the local GB structure adjustment at the GB segments I, II, and III, we need to get full insight into basic structural units at the GB, as shown in Fig. 4. Most structural units indicated by star-marked capital letters to differ from the common structural units[23,24] have become distorted. They are regarded as new structural units that have not been identified in idealized simulations and they are related to those idealized units. A*/C* structural unit is a rotated and distorted A/C structural unit which is made of four atoms placed in diamond. C** has one more atom than C* structural unit. According to the relationship between the atoms of the structure unit and the two neighboring grains, we can differentiate A* and C* structural units, i.e. two atoms of the C* structural unit belong to each neighboring grain, while three atoms of the A* structural unit belong to one grain. B* structural unit has one more atom than a rotated

https://doi.org/10.1557/mrc.2016.10 Published online by Cambridge University Press

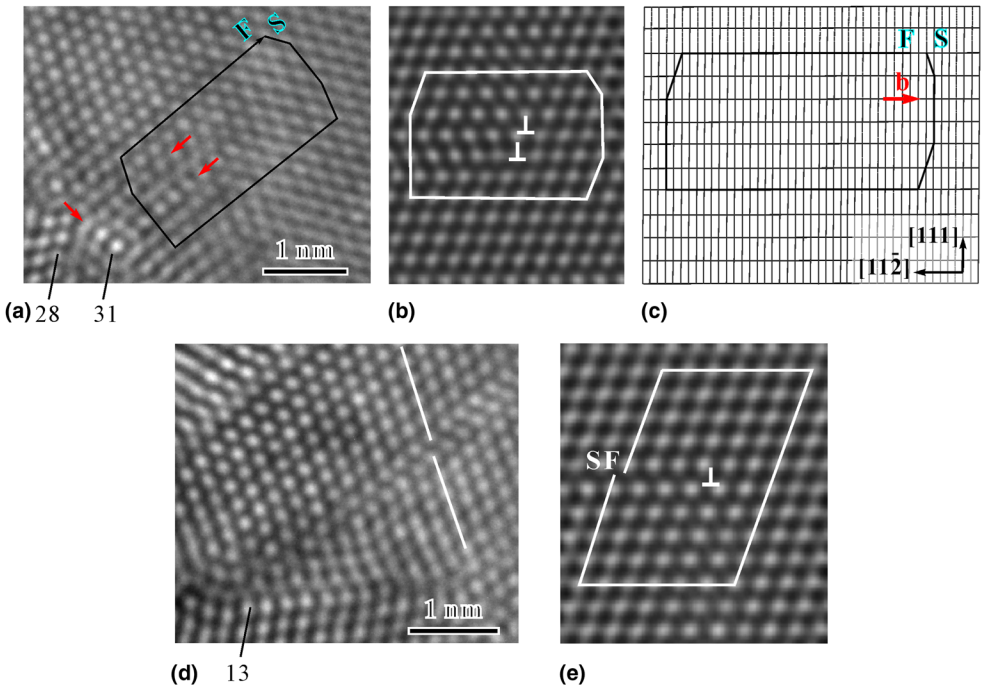


Figure 3. HREM observations of the newly formed twin and the partial dislocation: (a) Close observation of the area around the GB segment ranging from No. 28 to 31 in Fig. 1(d) and the Burgers circuit path about the defect is marked. The newly formed TBs are indicated by the red arrows. (b) The simulated image of the area including partial dislocations and twin in (a) using the multislice method, showing the existence of two partial dislocations in the twin front. Simulation conditions are chosen as following: sample thickness 5.1 nm and defocus value −70 nm. The local sample inclination induced by deformation was not taken into account. (c) Schematic illustration of Burgers circuit (FS/RH convention) in displacement shift complete (DSC) reference lattice. Lines along [11$\bar{2}$] and [111] directions are spaced at intervals of $\frac{a}{12}$[11$\bar{2}$] and $\frac{a}{3}$[111], respectively. (d) Close observation of the area in the GB segment around No. 13 in Fig. 2(c) shows the existence of a stacking fault indicating the emission of a Shockley partial dislocation, as evidenced by the white lines. (e) The simulated image of a partial dislocation and a stacking fault (SF) behind.

and distorted B structural unit which connects eight atoms by a polygon and one atom inside the polygon. E* structural unit has one more atom inside the unit than a rotated and distorted E structural unit which has a mirror symmetry across the interface. GB segment III initially consisted of repeated C* structural unit and a pentagon structural unit caused by the existence of the GBD1 (indicated by a circle) near the junction [No. 13 in Fig. 4(a1)]. Then, GB segment III was transformed into that composed of the C* structural units, additional A* and E* structural units with increasing time [see Figs. 4(a1)–4(a3)]. Especially, the GBD1 moved toward the triple junction and hardly advanced further due to the block of the well-ordered facet in Fig. 4(a3), which caused a partial dislocation to emit from the junction. Here, the local atom shuffling at the GB assisted the change in shape of the structural units and allowed creation of the necessary Burgers vector for the Shockley partial dislocation.[10,11] For GB segment II, the (1 1$\bar{5}$)/(1 1$\bar{1}$) boundary [Fig. 1(b)] constituting of repeated B* structural units [Fig. 4(b1)] moved toward **G2** without losing the atomic-scale facet structure [Fig. 4(b2)]. Then, the GBD6 [indicated by a circle in Fig. 4(b3)] moved across the **T11** boundary (No. 36) and the GB junction, causing one B* structural unit [Fig. 4(b2)] transformed into the C* structural unit [Fig. 4(b3)]. For the GB segment I, the initially stepped ($\bar{3}$, $\bar{3}$, 1 1)/(1 1$\bar{1}$) facet from No.14 to No. 20 has moved toward **G2** and the GBD2 moved out of the facet, which made the stepped facet elongated about three atom columns [Figs. 4(c1)–4(c3)]. Another two facets (1 1$\bar{5}$)/(1 1$\bar{1}$) and (1 1$\bar{5}$) facets in Fig. 1(b)] lost their facet structures during GB migration [Figs. 4(c1)–4(c3)]. Especially, the (1 1$\bar{5}$) facet was transmitted into a Σ3 coherent TB indicated by the D structural unit in Figs. 4(c1)–4(c3), during the GB dissociation. At the same time, the GBDs 2–6 all moved toward right in the GB, indicating that the delocalization of the GBDs greatly changed the local GB structures.

Discussion

The main finding was the evident adjustment ability of the local GB structures during GB migration, which involved five types of GB-related behaviors (i.e., GB dissociation, partial dislocation emission from GB, faceting/defaceting, and GBD motion). These GB-related behaviors were influenced by the local GB structures (the basic structural units), and in turn also modified the GB structures to accommodate GB migration.

https://doi.org/10.1557/mrc.2016.10 Published online by Cambridge University Press

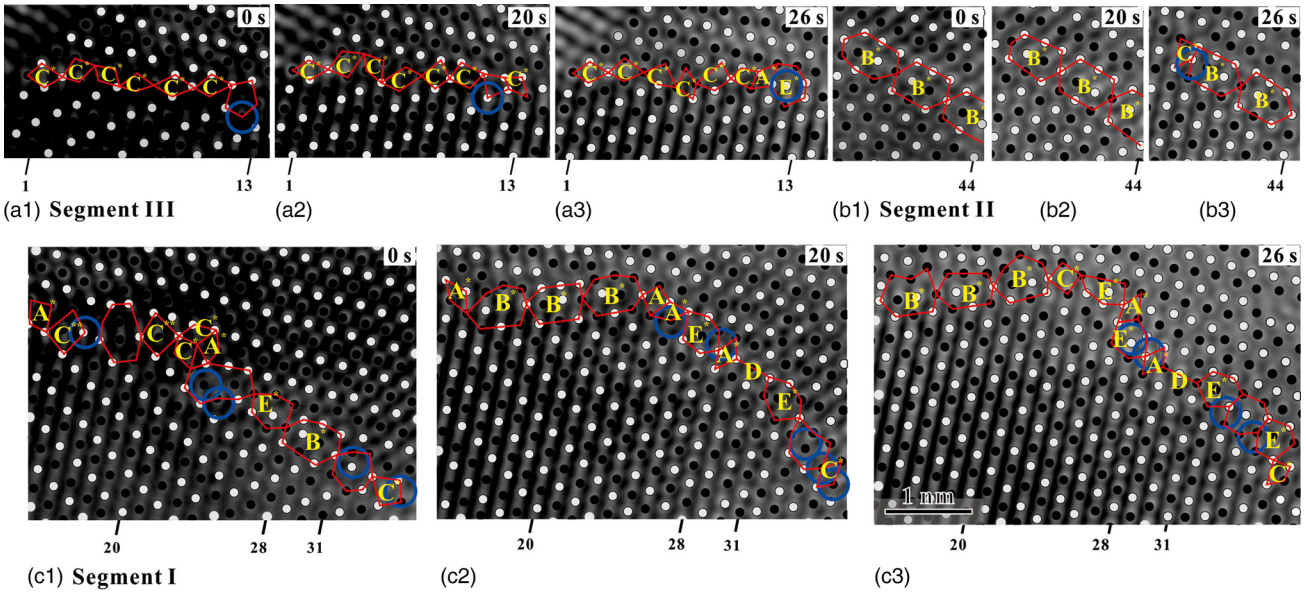


Figure 4. Evolution of the GB structural units and the GBDs during GB migration: Each GB structural unit is indicated by the red polygon, and the GBDs are indicated by the blue circles. (a1–a3) for segment III and GBD 1, (b1–b3) for segment II and GBD 6, and (c1–c3) for segment I and GBDs 2–6 (counting sequence from left to right). The white and black atoms indicate that they are on the different {200} planes.

Firstly, we would figure out the driving force for GB migration. Previous in situ experiments have proved that extensive GB migration can happen only in the presence of applied driving force.[14,15] In the absence of strong driving force, the lattice regions were observed to fluctuate back and forth.[14,15] The observed GB migration in our experiments was irreversible, which needed extra driving force. In thermal-driven GB migration, GB tends to get smooth (like faceting) to get a low-energy state[25] or GB migrates toward its center of the curvature, in response of curvature or capillarity driving force.[26] Here, the GB moved in the opposite direction to the curvature center. Besides, both faceting and defaceting were observed. Thus, there should be an athermally driven force for GB migration.

Here, we need to consider the effects of electron irradiation, GB energy reduction, and strain/stress. Main effects of electron beam irradiation considered are heating, displacement damage, and sputtering.[27] Our HRTEM observations were performed at 200 kV with the current density of about 4.8 A/cm^2. Most electrons go through a thin specimen and lose very little energy under such current density, so the radiation heating can generally be neglected.[27] Although the energy of the electron beam (200 keV) is lower than the threshold energy (higher than 420 keV) for atom displacements,[27] atomic surface diffusion and possible vacancy/interstitial formation may well be enhanced under electron irradiation.[15] Such processes, therefore, could provide the necessary activation for GB migration at ambient temperatures.[14,15] In addition, the GB energy change during GB migration also made a contribution. For example, the driving force[22] for the GB dissociation $\Delta P = 2(\gamma_1/R_1 - \gamma_2/R_2)$, where $R_1 \approx R_2 = 1.94$ nm, $\gamma_1 = 704$ mJ/m^2, $\gamma_2 = 598$ mJ/m^2, where γ_1 and γ_2 are the GB energies of undissociated and dissociated Σ9 GB, respectively.[22] Thus, $\Delta P = 109$ MPa.

Irradiating solids with energetic particles does not always introduce an undesirable phenomenon,[28] sometimes, it may have beneficial effects, such as introducing driving force for high-pressure transformations of materials on the nanometer scale,[28] incoherent TB motion.[17] Direct measurement of the interplanar spacing was performed to estimate the strain/stress and strain energy in the present film. We estimated strain $\varepsilon = (d - d_0)/d_0$ using the ideal (111) interplanar spacing d_0 at room temperature and the actual (111) interplanar spacing d measured from the HRTEM images. We found that the strain in **G2** (ε~0.67%) was two times higher than that in **G1** ($\varepsilon \sim -0.21\%$), and **G1** had a more stable strain. Thus, GB migrated from **G1** into **G2** due to the gradient of elastic energy across a GB.[18] The origin of strain may come from sputtering-induced mass loss from the thinnest hole edge of the TEM sample. Such mass loss may change the local shape of the sample, which would introduce large internal stress. Although it would be arguable that the precision of HRTEM may not be sufficient to differentiate a 0.6% versus −0.2% difference, the possible mechanical driving force should not be ignored. The observed GB migration might be a stress-enhanced diffusion-dominant process.

Secondly, we would explain why there is a difference in the migrating distance of the three GB segments [Fig. 2(d)]. Based on the atomic-scale observations, we calculate the maximum normal GB migration velocity as a function of the GB inclination angle (φ) and present the corresponding GB adjustment behaviors in Fig. 5(a). As we known, GB mobility is dependent on GB misorientation. In addition to misorientation, GB

https://doi.org/10.1557/mrc.2016.10 Published online by Cambridge University Press

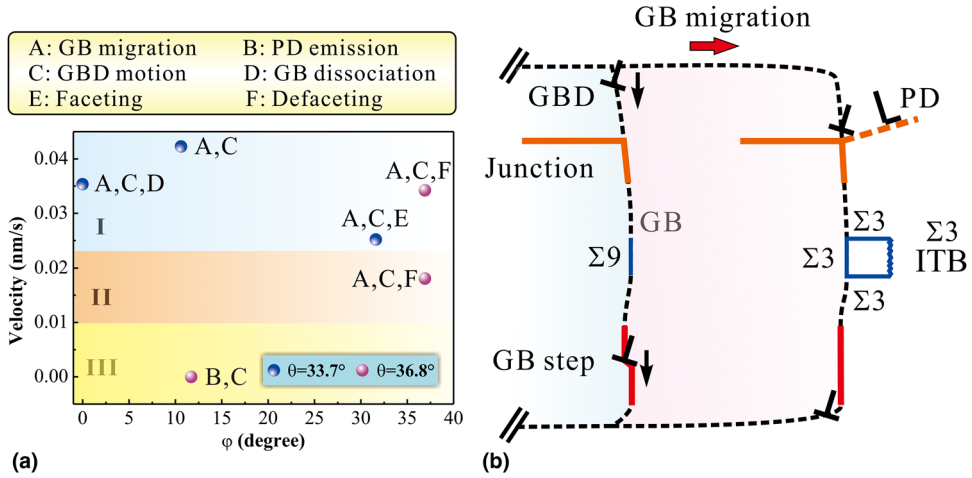


Figure 5. Relationship among local grain boundary structures and the grain boundary behaviors: (a) The figure shows the maximum normal GB migration velocity as a function of the GB inclination angle (ϕ). GB-related behaviors are marked on the corresponding GB structures. In the measurement of the GB inclination angle, the reference GB for the 33.7° ⟨110⟩ GB (blue points) and 36.8° ⟨110⟩ GB (pink points) is {115} and {114} STGBs, respectively. (b) A schematic illustration of the different GB-related behaviors during GB migration, including **B**: partial dislocation (PD) emission from the GB, **D**: Σ9 GB dissociation, and **E**: faceting. The dotted line presents the GB and the colored solid line indicates the GB segment where some GB-related behavior happens. "⊥" and "⌊" indicate the GBD and the PD, respectively. Σ3ITB presents Σ3 incoherent twin boundary.

mobility is also closely related to GB inclination and GBD distribution. We can see from Fig. 5(a) that the velocity of different GB fragments (presented by the filled circles) cannot be simply explained by the misorientation angle or GB plane (GB inclination), because even GBs with the same misorientation and inclination angle have different motion velocity. Thus, boundary models based on the geometrical consideration (like misorientation and inclination angles) are not suitable for understanding the nature of GB motion. To understand the different migration behavior, we introduce structural unit model, which is based on the thermodynamic principle that the free energy of the system is minimized.[29,30]

In Fig. 5, we can clarify the relationship among GB migration, GB adjustment behaviors and local GB structures, and their interaction, and summarize the key points. Firstly, most the GB-related behaviors listed in Fig. 5(a) are associated with the GBD motion, which indicates that GB adjustment behaviors were accommodated by the GBD motion. The collective motion of the atoms during GB migration allowed the motion of the GBDs. Atomic shuffling during the GBD motion allowed the formation of the Burgers vector of the emitted dislocation.[10,11] Figure 5(b) depicts the different GB-related behaviors during the GB migration process. Faceting is the process that a GB step or a GBD moved out the GB faceting, while defaceting is the process that GBDs move into the well-ordered GB. Σ9 GB has a special GB misorientation angle, which allows the existence of the triple junction Σ9–Σ3–Σ3. Besides, the Σ3 coherent twin boundary has quite low GB energy; thus GB dissociation Σ9 = Σ3 + Σ3 could be observed during the GB motion process. Secondly, the different local GB structures exhibit an evident difference in GB migration velocity. An evident migration ability of GB segment I is due to the fact that the GB segment contains both the hybrid structural units (different types of structural units) and the delocalized GBDs. In contrast, well-fit GBs with periodic structural units have lower GB migration velocity. The relative stability of the GB segments II and III results from the fact that these segments initially have the same type of structural units. Besides, the localized GBDs did not favor GB migration, like the GBD1 in the GB segment III. Our finding provides strong evidence to the previous simulation work[30,31] which suggests that a mechanically stable boundary is composed of a repeated sequence of the structural units. Our observations may explain that the macroscopic facets with high mobility may contain GBDs, while facets with low mobility have a more well-fit structure. Thirdly, the GB composed of the periodic structural units is effective in blocking the GBDs motion but enhances the possibility of the partial dislocation emission, as illustrated in Fig. 5(b). For example, the GBD1 blocked by the well-fit $(\bar{3}, \bar{3}, 1\,1)/(1\,1\,\bar{1})$ facet, caused the emission of the partial dislocation from the triple junction. It was reported that the emission of the partial dislocation from the triple point is energetically favorable.[32] Although the discussions on GB migration via several mechanisms are built upon HRTEM studies of a specific high-angle GB near two grains, our findings that local GB environment determines the GB behaviors have also been proved,[10,11,33–35] thus the observed GB-related behaviors are not an unusual phenomenon. Of course, further investigation on the GB migration behavior of other types of GBs to prove the general applicability is necessary.

In summary, abundant adjustment behaviors of the local GB structures were observed at the atomic scale during GB migration. GBs consisting of both "hybrid" structural units and delocalized GBDs are relatively unstable. Our observations reveal

https://doi.org/10.1557/mrc.2016.10 Published online by Cambridge University Press

the interaction of the GB-related behaviors and GB structures, and thus give direct experimental evidences for the numerous simulation results about the GB-related behaviors. Furthermore, the present results provide a fundamental solution to stabilize nanoGBs by means of a suppression of local GB structure adjustment through optimizing structural units. Thus, this may deepen the understanding of the strategies to stabilize the GBs through the pinning of particles/impurities and the nanoscale chemical segregation of the atoms to the unstable GBs.

Acknowledgments

This work was supported by the National Natural Science Foundation of China (NSFC, grant numbers 51371047 and 51571199), the External Cooperation Program of the Chinese Academy of Sciences (grant no. GJHZ1401), and partially supported by the NSFC (grant No. 51371180).

References

1. J. Schiotz and K.W. Jacobsen: A maximum in the strength of nanocrystalline copper. *Science* **301**, 1357 (2003).
2. V. Yamakov, D. Wolf, S.R. Phillpot, A.K. Mukherjee and H. Gleiter: Deformation-mechanism map for nanocrystalline metals by molecular-dynamics simulation. *Nat. Mater.* **3**, 43 (2003).
3. S.X. McFadden, R.S. Mishra, R.Z. Valiev, A.P. Zhilyaev and A.K. Mukherjee: Low-temperature superplasticity in nanostructured nickel and metal alloys. *Nature* **398**, 684 (1999).
4. X.M. Luo, X.F. Zhu and G.P. Zhang: Nanotwin-assisted grain growth in nanocrystalline gold films under cyclic loading. *Nat. Commun.* **5**, 3021 (2014).
5. T.J. Rupert, D.S. Gianola, Y. Gan and K.J. Hemker: Experimental observations of stress-driven grain boundary migration. *Science* **326**, 1686 (2009).
6. Y.T. Zhu, X.Z. Liao and X.L. Wu: Deformation twinning in nanocrystalline materials. *Prog. Mater. Sci.* **57**, 1 (2012).
7. K.S. Kumar, S. Suresh, M.F. Chisholm, J.A. Horton and P. Wang: Deformation of electrodeposited nanocrystalline nickel. *Acta Mater.* **51**, 387 (2003).
8. V. Yamakov, D. Wolf, S.R. Phillpot and H. Gleiter: Deformation twinning in nanocrystalline Al by molecular-dynamics simulation. *Acta Mater.* **50**, 5005 (2002).
9. X.L. Wu and E. Ma: Deformation twinning mechanisms in nanocrystalline Ni. *Appl. Phys. Lett.* **88**, 061905 (2006).
10. H. Van Swygenhoven, P. Derlet and A. Hasnaoui: Atomic mechanism for dislocation emission from nanosized grain boundaries. *Phys. Rev. B* **66**, 024101 (2002).
11. P.M. Derlet, H. Van Swygenhoven and A. Hasnaoui: Atomistic simulation of dislocation emission in nanosized grain boundaries. *Phil. Mag.* **83**, 3569 (2003).
12. L.E. Murr: Strain-induced dislocation emission from grain boundaries in stainless steel. *Mater. Sci. Eng.* **51**, 71 (1981).
13. B.B. Straumal, S.A. Polyakov and E.J. Mittemeijer: Temperature influence on the faceting of Σ3 and Σ9 grain boundaries in Cu. *Acta Mater.* **54**, 167 (2006).
14. K.L. Merkle, L.J. Thompson and F. Phillipp: Collective effects in grain boundary migration. *Phys. Rev. Lett.* **88**, 225501 (2002).
15. K.L. Merkle and L.J. Thompson: Atomic-scale observation of grain boundary motion. *Mater. Lett.* **48**, 188 (2001).
16. K.L. Merkle, L.J. Thompson and F. Phillipp: In-situ HREM studies of grain boundary migration. *Interface Sci.* **12**, 277 (2004).
17. L. Liu, J. Wang, S. Gong and S. Mao: High resolution transmission electron microscope observation of zero-strain deformation twinning mechanisms in Ag. *Phys. Rev. Lett.* **106**, 175504 (2011).
18. G. Gottstein and L.S. Shvindlerman: *Grain Boundary Migration in Metals: Thermodynamics, Kinetics, Applications*, 2nd ed. (CRC Press, Boca Raton, 2010).
19. C.T. Koch. Determination of core structure periodicity and point defect density along dislocations. Ph.D. Dissertation, Arizona State University, Tempe, AZ, 2002.
20. D.G. Brandon: The structure of high-angle grain boundaries. *Acta Metall.* **14**, 1479 (1966).
21. D.L. Medlin, C.B. Carter, J.E. Angelo and M.J. Mills: Climb and glide of a/3 ⟨111⟩ dislocations in an aluminium Σ = 3 boundary. *Phil. Mag. A* **75**, 733 (1997).
22. K.L. Merkle and D. Wolf: Low-energy configurations of symmetric and asymmetric tilt grain boundaries. *Phil. Mag. A* **65**, 513 (1992).
23. J.D. Rittner and D.N. Seidman: ⟨110⟩ symmetric tilt grain-boundary structures in fcc metals with low stacking-fault energies. *Phys. Rev. B* **54**, 6999 (1996).
24. M.A. Tschopp, G.J. Tucker and D.L. McDowell: Structure and free volume of ⟨110⟩ symmetric tilt grain boundaries with the E structural unit. *Acta Mater.* **55**, 3959 (2007).
25. Z. Horita, D.J. Smith, M. Furukawa, M. Nemoto, R.Z. Valiev and T.G. Langdon: An investigation of grain boundaries in submicrometer-grained Al–Mg solid solution alloys using high-resolution electron microscopy. *J. Mater. Res.* **11**, 1880 (1996).
26. F. Mompiou, M. Legros, T. Radetic, U. Dahmen, D.S. Gianola and K.J. Hemker: In situ TEM observation of grain annihilation in tricrystalline aluminum films. *Acta Mater.* **60**, 2209 (2012).
27. R.F. Egerton, P. Li and M. Malac: Radiation damage in the TEM and SEM. *Micron* **35**, 399 (2004).
28. A.V. Krasheninnikov and F. Banhart: Engineering of nanostructured carbon materials with electron or ion beams. *Nat. Mater.* **6**, 723 (2007).
29. H. Gleiter: The structure and properties of high-angle grain boundaries in metals. *Phys. Status Solidi b* **45**, 9 (1971).
30. A.P. Sutton and V. Vitek: On the structure of tilt boundary boundaries in cubic metals I. symmetrical tilt boundaries. *Phil. Trans. R. Soc. A* **309**, 1 (1983).
31. H. Zhang and D.J. Srolovitz: Simulation and analysis of the migration mechanism of Σ5 tilt grain boundaries in an fcc metal. *Acta Mater.* **54**, 623 (2006).
32. M.Y. Gutkin, I.A. Ovid'ko and N.V. Skiba: Emission of partial dislocations from triple junctions of grain boundaries in nanocrystalline materials. *J. Phys. D., Appl. Phys.* **38**, 3921 (2005).
33. H. Van Swygenhoven and P. Derlet: Grain-boundary sliding in nanocrystalline fcc metals. *Phys. Rev. B* **64**, 224105 (2001).
34. D.E. Spearot, K.I. Jacob and D.L. McDowell: Dislocation nucleation from bicrystal interfaces with dissociated structure. *Int. J. Plasticity* **23**, 143 (2007).
35. P.M. Derlet, A. Hasnaoui and H. Van Swygenhoven: Atomistic simulations as guidance to experiments. *Scr. Mater.* **49**, 629 (2003).

https://doi.org/10.1557/mrc.2016.10 Published online by Cambridge University Press